An Experimental Study of Hypersonic Wakes behind Wedges at Angle of Attack

JIUNN-JENQ WU* AND WILHELM BEHRENS†
California Institute of Technology, Pasadena, Calif.

Experimental measurements of mean flow properties of hypersonic wakes behind wedges of 20° included angle were conducted for angles of attack up to 25° at Mach number 6, with Reynolds number based on wedge base height ranging from 7000 to 55,000. The near and far wake structures were determined, including streamlines and velocity profiles, over a downstream distance of 60 base heights. The base pressure changes as a function of Reynolds number and angle of attack, especially for $\alpha > 17°$, and $Re_{\infty,H} > 14{,}000$. Separation on the leeward surface occurs at $\alpha > 17°$. The near wake flowfield changes accordingly. The far viscous wake ($x/H > 4$) changes with increasing incidence because of the increasing differences of the inviscid flow quantities at the leeward and windward edges of the viscous wake. The wake static pressure as measured by its maximum value at $x \simeq 20H$, increases with incidence. The wake pressure, and the viscous wake edge velocities, the edge temperatures, and the flow inclination of the experimental flow (directed toward the leeward side) compare favorably with a simple inviscid shock expansion model. In the laminar wake flows the wake widths, minimum velocities, and maximum temperatures change little with incidence. However, in the transitional wake flows, the "breakaway" phenomenon is observed and transition from laminar to turbulent flow moves upstream as angle of attack increases.

Nomenclature

H = total base height
M = Mach number
P = Pressure
P_{t2} = Pitot pressure
$Re_{\infty,H}$ = Reynolds number based on freestream conditions and base height
T = temperature
U = streamwise velocity
V = transverse velocity
x = streamwise coordinate
y = transverse coordinate
α = angle of attack
ρ = density
ψ = streamline $\left(= \int_o^y \rho U \, dy\right)$

Subscripts

b = base
e_1 = leeward edge of viscous wake
e_2 = windward edge of viscous wake
H = base height
o = reservoir condition
t = local stagnation quantity
TR = transition
∞ = freestream condition

Introduction

GREAT efforts have been made in the last decade trying to understand hypersonic wakes. The problems encountered in hypersonic wakes and progress made until 1964 were discussed in a paper by Lees.[1] A review of later developments was given by Lykoudis.[2] Because of the complex nature of this subject, most of the detailed experimental flowfield studies were limited to wakes of nonlifting, two-dimensional[3-6] and axisymmetric bodies.[7,8] Theoretical studies were carried out at the same time.[9-11] In many cases re-entry bodies are nonsymmetric or are flying at angles of attack.[12]

A distinction should be made between axisymmetric and two-dimensional bodies at angle of attack. Experimental studies of flows over cones at angle of attack[13] show that a very thick boundary layer develops on the leeward side even at relatively small angles of attack. Consequently, in the near wake the steeper gradients in velocity and temperature occur on the windward side[14] and not on the leeward side where they occur in the wake flow of a wedge at angle of attack. Hence, the wake flows of axisymmetric and two-dimensional bodies at angle of attack are qualitatively different. Only two-dimensional wake flows of wedges will be discussed in this paper.

Relatively little is known about these wake flows. There is still a lack of understanding of how sensitive the near wake is to angles of attack. For example, when do changes that occur in the base region affect the flow on the leeward side of the body, how does a "large" angle of attack affect the near wake (base pressure, wake neck and rear stagnation point location, shear flow profiles), and the far wake flowfield (inviscid flow, static pressure distributions, viscous wake growth and velocity profiles) and does an angle of attack affect transition from laminar to a turbulent wake flow?

These are questions which were studied in the present experimental investigation of the flow at Mach 6 over two-dimensional 20° wedges at angles of attack up to 25°. This body-shape was chosen because careful near and far wake flowfield results for the same wedges at zero angle of attack were available (Batt and Kubota[6]).

In order to find out what effect an angle of attack has on the overall flowfield, a simple shock expansion model was employed to estimate the inviscid flowfield. In 1948, Kahane and Lees[15] calculated the inviscid flowfield about a two-dimensional flat plate at small angle of attack, moving at supersonic speeds. They found, somewhat surprisingly, that there was an upwash directly behind the trailing edge of the airfoil. For flows over wedges the inviscid flow is undetermined unless the base pressure is specified. For a given (assumed) base pressure the inviscid flow, consisting of oblique shocks and Prandtl-Meyer expansions, was calculated, as indicated in Fig. 1. On the windward side, there is an oblique shock on the leading edge, followed by a Prandtl-Meyer expansion, expanding the flow to the given base pressure and a sub-

Presented as Paper 71-563 at the AIAA 4th Fluid and Plasma Dynamics Conference, Palo Alto, Calif., June 21–23, 1971; submitted July 19, 1971; revision received July 10, 1972. This work was carried out under the sponsorship and with the financial support of the U. S. Army Research Office and the Advanced Research Projects Agency under Contract DA-31-124-ARO(D)-33.

Index categories: Supersonic and Hypersonic Flows; Jets, Wakes, and Viscid-Inviscid Flow Interactions.

* Graduate Student.

† Assistant Professor of Aeronautics. Member AIAA.

sequent oblique shock (wake shock) compresses the flow to the wake pressures and wake flow direction. This last compression is found by matching the wake pressures and flow directions of the two flows coming from the windward and leeward sides. The example of the resulting inviscid flowfield, given in Fig. 1, shows the flow over a 20°-wedge at Mach number 6 and at angle of attack of 15°.

As in the case of the flat plate at angle of attack there is an upwash, as indicated by the angle the slip-line makes with the freestream direction, $\delta_{slip} = 1.19°$. Because the air flow on the windward and leeward sides passes through shocks of different strengths, there is a slip-line in the wake across which velocity and temperature jump considerably ($u_{e2}/u_{e1} < 1$, $T_{e2}/T_{e1} > 1$). It is expected, therefore, that the viscous wake beyond the wake neck, formed from the coalescence of the free boundary layers which have separated from the wedge at or ahead of the base, differs from the symmetric wake because of the differences in inviscid flows at the leeward and windward edges of the viscous flow. An indication of this effect is given in Fig. 2 where pitot pressure traces across the wake of a wedge at angle of attack of 15° are shown.

In the near wake the situation is more complicated. Because of viscous-inviscid flow interaction near the leading edge of the models, a shock wave was observed on the leeward side even when the leeward side was inclined away from the freestream and the inviscid flow model would predict an expansion (Fig. 1). The flow on the leeward side of the wedge and in the near wake region is dominated by viscous-inviscid flow interactions.

A description of the measurements and experimental techniques and a discussion of the data reduction is given in the next section. Thereafter, results are presented and discussed, followed by a summary. More details of the results obtained in this study are given in Ref. 16.

Experimental Techniques and Data Reduction

The experimental work reported herein was conducted in the GALCIT Hypersonic Wind Tunnel. This tunnel is a continuous flow, closed return tunnel with a 5-in. × 5-in. test section and a nominal Mach number of 6. Models were placed about 23 in. downstream of the nozzle throat. This arrangement permitted wake measurements to approximately 10 in. downstream of the model. Freestream Reynolds numbers of 0.465, 0.94, 1.42 and 1.9×10^5 in. were selected for tests and a reservoir stagnation temperature of 275°F was always maintained.

The models were two wedges of 20° included angle with respective base heights of 0.15 in. and 0.3 in. They were originally used by Batt and Kubota[6] in their surveys of hypersonic wakes behind wedges at zero angle of attack. Both models spanned the wind tunnel. Their leading edges were carefully machined to a thickness of less than 0.002 in. The wedge model with a base height of 0.3 in. had four surface pressure taps and one base pressure tap. A shaft was located 0.25 in. from the base. The second model used was a wedge with 0.15 in. base height. This model had two pressure taps installed on the centerline of the wedge base. A shaft was located 0.20 in. from the base. These two wedges could rotate around their shafts. Angles of attack were indicated by metal arms attached to the shafts. All locations were measured relative to the center of the base when the wedges were at zero angle of attack (see Fig. 2).

The question of two-dimensionality of base and wake flow has been studied extensively at GALCIT by previous authors[4,6] for similar model configurations in the same wind tunnel. In the present experiments two-dimensionality has been established by following those authors in the model setups. The models spanned the test-section and had aspect ratios (span/model height) of 16.7 and 33.3. One good check on two-dimensionality was that for the two models, the base pressure at the same Reynolds number compared very well. When separation occurred on the leeward side the oil flow experiments showed a separation line parallel to the trailing edge within the central $3\frac{1}{2}$ in. All data

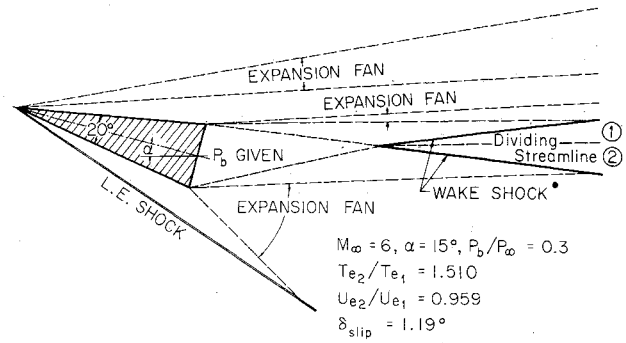

Fig. 1 Typical results from inviscid flow model (shock-expansion theory).

presented in this paper are considered reasonably two-dimensional.

Static pressure distributions in the wake were measured by a silicone micromanometer using a cone-cylinder static pressure probe fabricated from a 0.032 in. stainless-steel tubing, similar to the probe designed and calibrated by Behrens.[17] Those calibration results were applied to correct the measured data for viscous interaction effects. Static pressure measurements were made only in regions where the flow angle was less than 5° with respect to the probe axis as checked a posteriori. The error of the static pressure measurement within this angle of attack is estimated to be less than ±4%.

Pitot pressure surveys were performed using a probe flattened to 0.030-in. × 0.003-in. opening at the forward end. The effect of angle of attack of the probe with respect to the local flow direction was checked. As measured by McCarthy,[18] for flow inclinations up to 15°, the error of measurements was less than 1% and only 4% at 25°. In the present experiments for the largest angle of attack (25°) with a flow inclination of 35°, the measured Pitot pressure behind the leading edge shock was 8% less than the calculated value. Since most flow inclinations encountered in the present experiments were far below 35°, the error in pitot pressure caused by mis-alignment of the pitot probe was small. A 0–5 psi Statham pressure transducer was used to convert pressure measurements to electrical signals. Probe position and pitot pressure were recorded on a Moseley *XY* recorder. The flow separation on the leeward surface of the model was determined by applying a thin coat of oil.

Three independent flow parameters have to be known in order to reduce the raw data to primary variables. These independent parameters were 1) measured pitot pressure, 2) assumed constant

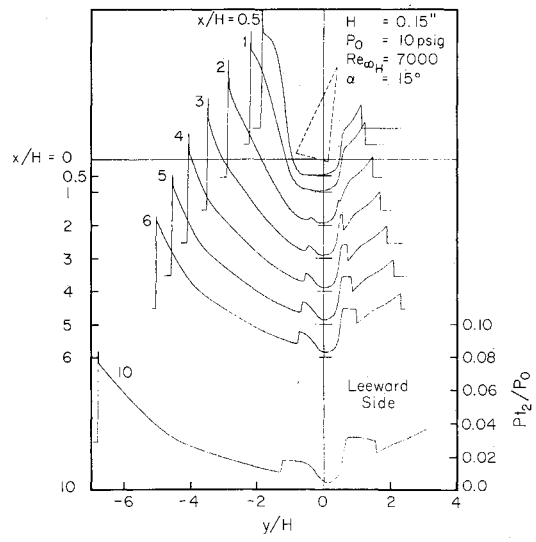

Fig. 2 Pitot pressure traces across the wake for an angle of attack of 15°.

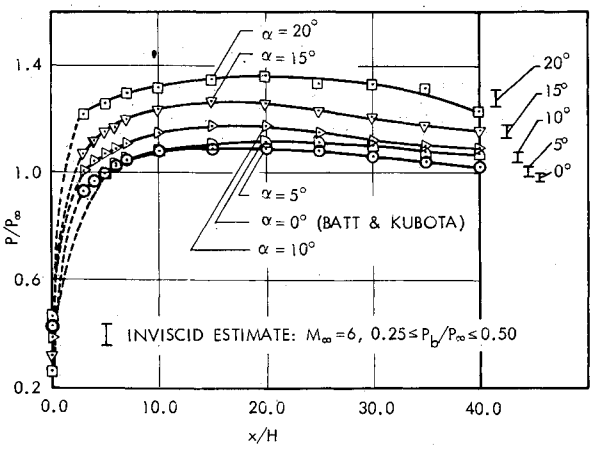

Fig. 3 Streamwise static pressure traces for several angles of attack at $Re_{\infty,H} = 7000$ ($H = 0.15$ in.).

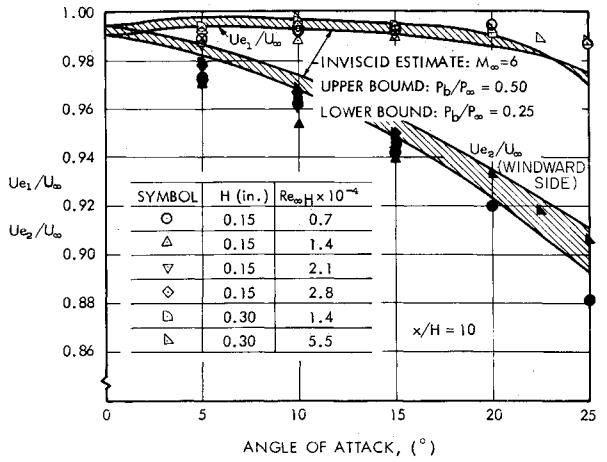

Fig. 5 Viscous wake edge velocities: comparison of measured velocities at $x/H = 10$ with theoretical results.

total temperature equal to its freestream value, 3) measured static pressure in the viscous wake or stagnation pressure determined from the slope of the shock wave in the inviscid wake. In the near wake flows, the viscous region extends beyond the wake shock waves; Pitot pressure jumps across these shock waves were used to evaluate the static pressure jumps. Since the static pressure is known inside the wake shock, it could be calculated ahead of the shock.

Near wake streamlines were constructed by integrating the mass flux from the leeward side leading edge shock wave toward and across the viscous wake.[6] Far wake streamlines were constructed in a different fashion, since the leading edge shock was outside the range of measurement. When the pressure gradient is negligible and the boundary-layer equations are applicable, an integral of the momentum equation is

$$\frac{d}{dx}\int_{y_{e_2}}^{s} \rho U(U_{e_2} - U)\,dy + \int_{s}^{y_{e_1}} \rho U(U_{e_1} - U)\,dy = \rho(U_{e_1} - U_{e_1})\left(V - U\frac{ds}{dx}\right)\Bigg|_{y=s} \quad (1)$$

where $U = U_{e_{1,2}}$ at $y_{e_{1,2}}$. The right-hand side of Eq. (1) vanishes if $ds/dx = V/U$ which means that $y = s(x)$ is a streamline. Consequently, along the streamline $y = s(x)$, Eq. (1) may be integrated and becomes

$$I = \frac{1}{\rho_\infty U_\infty^2 H}\left[\int_{y_{e_2}}^{s} \rho U(U_{e_2} - U)\,dy + \int_{s}^{y_{e_1}} \rho U(U_{e_1} - U)\,dy\right] \quad (2)$$

This invariant along a streamline served as a tool to construct far wake stream lines.

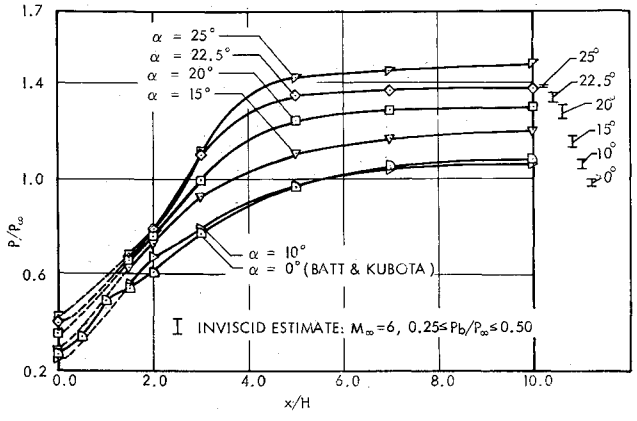

Fig. 4 Streamwise static pressure traces for several angles of attack at $Re_{\infty,H} = 55{,}000$ ($H = 0.30$ in.).

Results and Discussion

The portion of the wake upstream and including the wake neck is defined as the near wake, while the wake downstream of the neck in the region where the wake shocks are well formed and the pressure is constant across the wake is considered the far wake ($x/H \gtrsim 4$).

Far Wake Flowfield

Pressure Field and Viscous Wake Edge Flow Parameters

Pressure field

Static pressure measurements at the location of minimum pitot pressure are shown in Fig. 3 ($H = 0.15$ in.) and Fig. 4 ($H = 0.30$ in.) as function of angle of attack for Reynolds numbers $Re_{\infty,H} =$ 7000 and 55,000. The static pressure is reasonably constant across the viscous wake, so that the measurements presented here are the proper viscous wake static pressures.

In all cases tested the streamwise static pressure data indicate an initial overshoot followed by a gradual decay back to free-stream conditions. The overshoot depends very strongly on angle of attack; the higher the angle of attack, the larger the overshoot.

The effect of Reynolds number on the overshoot was discussed by Batt and Kubota[6] in their symmetric wake experiments. Their experiments showed that the lower the Reynolds number, the higher the overshoot. Similar results were found in the present tests but the effect of angle of attack is much stronger than that of Reynolds number.

The overshoot in static pressure as function of angle of attack may be explained by a simple inviscid shock-expansion model which was discussed in the introduction. First, however, the viscous wake edge results will be presented, since they also may be calculated using the same model.

Viscous Wake Edge Properties

In the far wake ($x/H \gtrsim 4$) where the wake shocks are well formed, the pitot pressures are at two distinct levels on each side of the viscous wake (Fig. 2). The pitot pressure levels together with the measured static pressures (and $T_t = T_0$) yield the viscous wake edge quantities, such as velocities, temperatures and Mach numbers. Since the total temperature T_t is constant, the Mach number and static temperature may be directly calculated from the velocity. Hence, only the velocities are shown here. Note, however, a decrease of 8% in velocity at Mach number 6.1 changes the Mach number to 3.85 and increases the temperature by a factor of 2.1. Representative results of the measured edge velocities at $x/H = 10$ for angles of attack of 5 to 25° are given in Fig. 5. (The calculated velocities shown also in this Figure will be

discussed in the next Section.) The effect of Reynolds number is very small, yet a systematic decrease of windward velocity with decreasing Reynolds number is perceptible.

The edge values of velocity, Mach number and temperature on the leeward side for all angles of attack are very close to the freestream values. However, on the windward side these quantities change considerably with angle of attack. The velocity and Mach number decrease and the temperature increases with angle of attack. At all angles of attack the edge velocity and Mach number increase slightly as the flow moves downstream, indicating a slow expansion of the wake flow in the region behind the wake shocks. Compared to the changes taking place inside the viscous wake these slight gradients at the edges of the viscous wake are very small.

Comparison of Experimental Wake Edge Flow Quantities with Inviscid Flow Calculations

Even though the real flow over the wedge is quite different, the simple inviscid shock expansion model, mentioned in the introduction and shown in Fig. 1, has been used to calculate the wake static pressure and the velocities and temperature levels outside the viscous wake. The purpose of making a comparison of the measured flow quantities with the computed values is to show that the main effect of angle of attack in the far wake is on the inviscid wake flow quantities. For the comparison to be meaningful the computed results should be compared with measured flow quantities at a location where the static pressure has reached a plateau which should be mainly determined by the inviscid flow structure. The measured static pressure maxima were found to be near $x/H \simeq 20$. Thereafter, as expected, the static pressure decreases slowly (Fig. 3). As discussed in the previous section the measured viscous wake edge quantities change little between $20 \leqq x/H \leqq 60$.

The base pressures of $P_b/P_\infty = 0.25$ and 0.5 are chosen as reasonable estimates of base pressures for the present inviscid calculation. This choice is consistent with the present range of base pressure measurements. Since the static pressures were found to be nearly constant across the viscous wake, the measured wake pressure levels (maximum values found in the wake) are compared with the computed values in Fig. 3 and 4. The calculated pressures certainly show the proper trend. The wake pressure level is quite insensitive to the base pressure level. The edge velocities as function of angle of attack are compared with the inviscid calculation in Fig. 5. Close agreement between measured and calculated velocities was found.

From the inviscid calculation, the inclination of the wake dividing streamline may be obtained. It is shown in Fig. 6 as function of angle of attack. This figure also includes the results inferred from the measurements ($20 \leqq x/H \leqq 60$). Again, good agreement between experiment and the theoretical model is demonstrated. Note that the wake flow inclination is directed towards the leeward side.

The close correspondence between the simple inviscid shock-expansion model and the real wake flow outside the viscous wake for $M_\infty = 6$, $\alpha \leqq 25°$ indicates that the inviscid far wake flow is determined mainly by the relative strengths of the leading edge shocks and the fact that the flows at the edges of the viscous wake have to be nearly parallel to each other. Its dependence on the base flow, i.e., on base pressure and Reynolds number is very weak. Because of separation on the leeward model surface and substantial changes of the "effective body" associated with separation, this simple inviscid model appears to become less accurate at angles larger than 25°.

Viscous Wake Width and Minimum and Maximum Properties

The location of wake edges were determined by the intersection of the tangent of the maximum transverse gradients and the wake edge levels of the pitot pressure traces. The wake thickness was obtained by measuring the distance between these intersections on the leeward and windward sides. Since the profile shapes

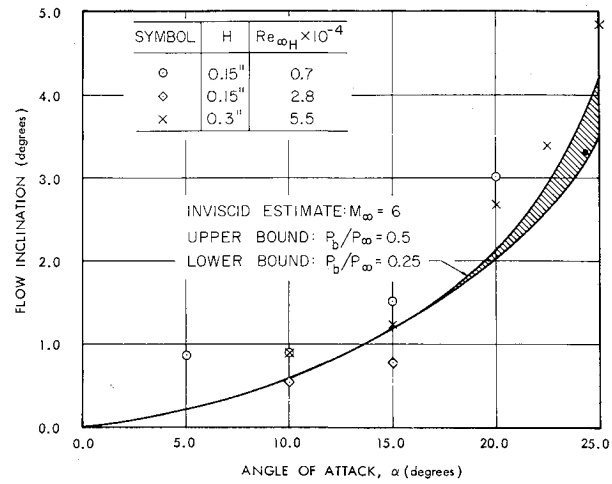

Fig. 6 Far wake slipstream inclination: comparison of measured dividing streamline inclination with inviscid calculation.

change with angle of attack this method of measuring the wake width does not yield high accuracy in the absolute magnitude of the wake width but of the growth rates which are important. Figure 7 shows wake widths for a Reynolds number of 55,000. The wake widths grow nearly linearly and indicate only a very small effect of angle of attack up to $\alpha = 15°$. However, from a certain point on, the wake growth is much faster than ahead of this point. This "breakaway" phenomenon has been observed before in symmetric hypersonic wakes by Behrens[5] and Batt and Kubota.[6] It is interpreted as the onset of a nonlinear instability which is also called the onset of transition, where because of the finite fluctuations. the Reynolds stresses start to become important and the mean flow starts to grow faster than a laminar steady wake flow.

From these results it is concluded that in the present experiments the wakes at the two lower Reynolds numbers ($Re_H =$ 7000 and 14,000 are laminar within the region of measurement and that at the two larger Reynolds numbers ($Re_{\infty,H} = 28{,}000$ and 55,000) at some station in the wake the onset of a nonlinear instability (transition) occurs. This onset of transition moves toward the wedge model as angle of attack is increased (see section on "Transition").

Minimum Velocities and Mach Numbers and Maximum Temperatures

The minimum velocities and maximum temperatures which are the properties on the wake centerline for the wake without angle of attack exhibit similar trends as the wake widths.

At the two lowest Reynolds numbers ($Re_{\infty,H} = 7000$ and 14,000) the minimum velocities change very little with angle of

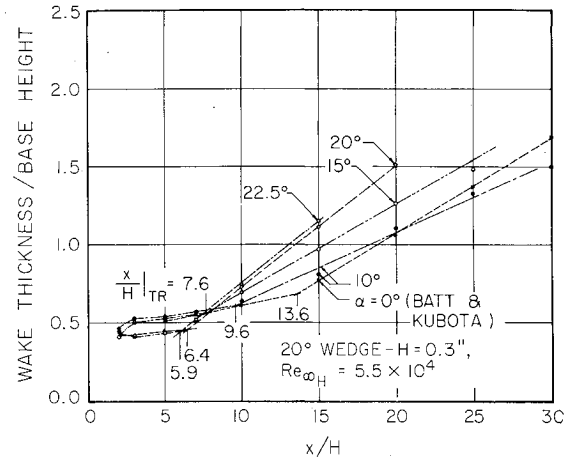

Fig. 7 Wake thicknesses as function of angle of attack.

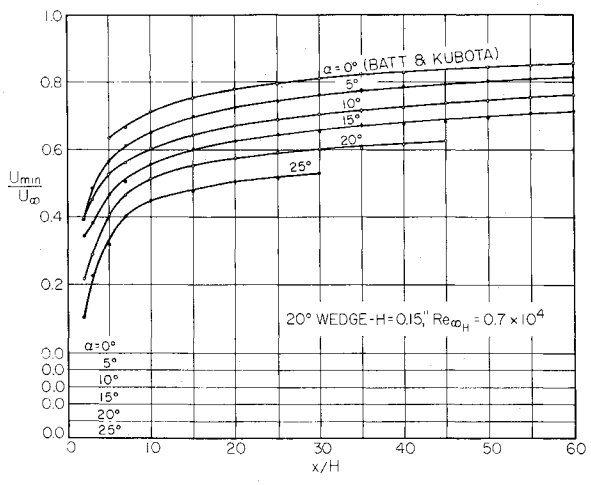

Fig. 8 Minimum velocity as function of angle of attack.

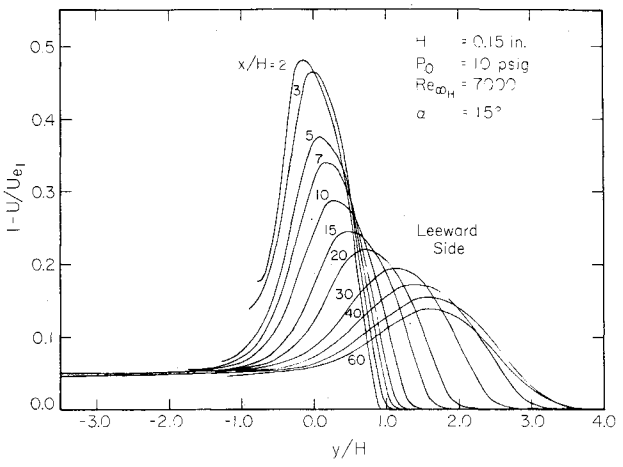

Fig. 10 Normalized velocity defects (laminar wake).

attack (Fig. 8). At the larger Reynolds numbers the deviation from the minimum velocity growth rate of a laminar steady wake occurs somewhat sooner than would be predicted by the growth of the wake widths. This earlier rise of the wake centerline quantities compared to the growth rate of the wake widths was already observed by Batt and Kubota[6] in their studies of symmetric wakes. At the Reynolds numbers of 28,000 and 55,000 also the minimum velocities exhibit growth rates from a certain point on that are faster than the growth rates of laminar wakes. Thus, the angle of attack does not affect the minimum quantities of the laminar wakes, but has an effect on transition.

Transition

The location of transition was determined from the sudden increase of growth rate of wake widths (Fig. 7).

In Fig. 9 the location of transition is presented as function of angle of attack for two Reynolds numbers, namely, $Re_{\infty,H}$ = 28,000 and 55,000. The results indicate that, for the same Reynolds number, transition moves upstream as the angle of attack is increased. This behavior of the wake may be explained qualitatively by linear instability theory. As indicated in the next section, the velocity gradient on the leeward side of the laminar viscous wake increases sharply as angle of attack is increased. It may be shown[19,20] that laminar wake profiles become more unstable when for a fixed wake thickness the maximum velocity gradient of the wake velocity profile increases, thus shortening the linear instability region and hence hastening transition (onset of nonlinearity) when the angle of attack is increased.

Far Wake Profiles and Streamlines

Mean wake profiles were calculated from the measured data. Two cases were selected for discussion: 1) $Re_{\infty,H} = 7000$, $\alpha = 15°$, $H = 0.15$ in.; and 2) $Re_{\infty,H} = 28{,}000$, $\alpha = 15°$, $H = 0.15$ in. In the first case the wake is laminar within the whole region of measurement (60 base heights). In the second case the onset of transition as defined in the last section occurs at $x/H = 16.5$. The velocity profiles are shown in Figs. 10 and 11.

In the wake regions ($x/H < 16.5$) where both wakes are laminar the profiles at the higher Reynolds number have much steeper gradients than in the lower Reynolds number case. Also, the gradients are steeper on the leeward side than on the windward side. A comparison with the measurements of Batt and Kubota[6] indicates that the gradients on the leeward side are not only larger than those on the windward side but are also larger than those of the symmetric wake.

These profiles also show that the nonsymmetric viscous wake is qualitatively composed of a "wake" component and a "free shear layer" component. In the transitional wake, the profiles at $x/H = 60$ are quite close to the profile shapes of a free shear layer.

Far wake streamlines were obtained by the method described in the Section on data reduction. The quantity "I" follows the notation given by Eq. (2), and is an invariant along a far wake streamline. The initial station for the far wake streamline calculation is $x/H = 5$. At this station the minimum velocity point is taken as the starting point of the approximate dividing streamline. Typical results of the far wake streamline calculations are presented in Fig. 12 in which the line of minimum velocity and the

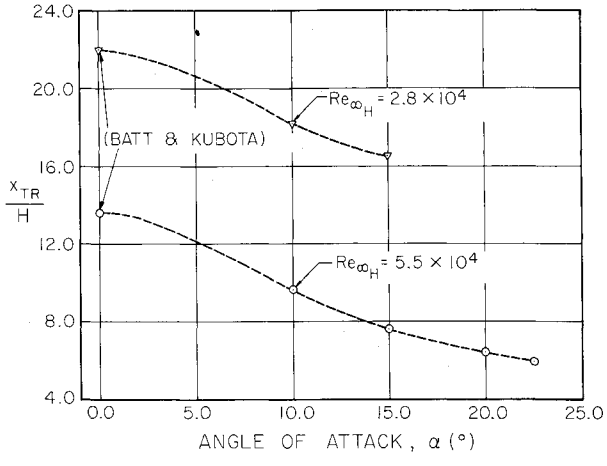

Fig. 9 Effect of angle of attack on transition.

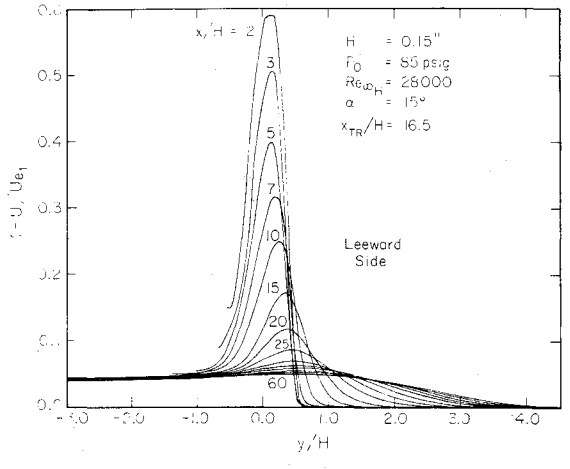

Fig. 11 Normalized velocity defects (transitional wake).

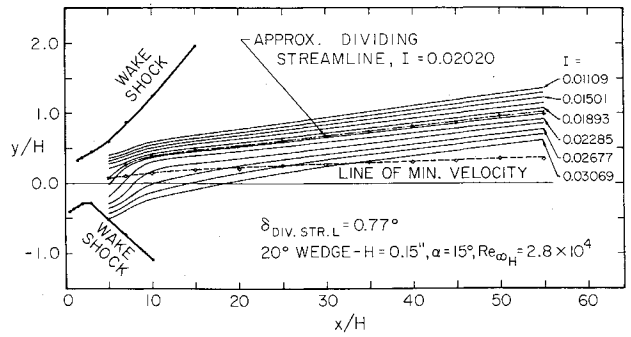

Fig. 12 Far wake streamlines.

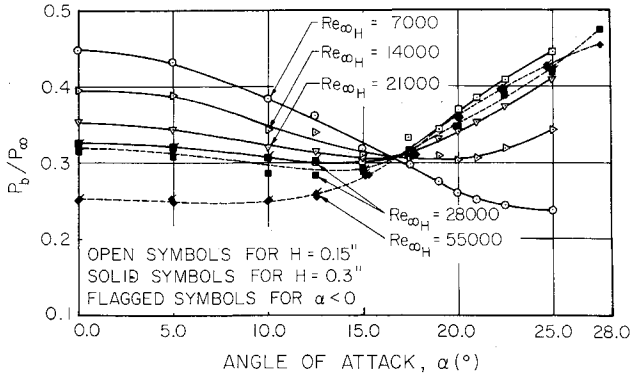

Fig. 13 Base pressure as a function of angle of attack and Reynolds number.

wake shocks are also included. The dividing streamline has a larger slope with respect to freestream than the line of minimum velocity. Note, however, $\delta_{Div.str.} = 0.77°$ only.

Laminar Near Wake Flow

Investigations of the near wake flow were limited by the dimensions of the static pressure probe being used in the present test. However, an approximation of static pressure in the small base flow region could be obtained by interpolating the base pressure and the closest downstream static pressure measured with the present static pressure probe.

Base and Surface Pressures

Base pressure measurements for both wedges as function of angle of attack are presented in Fig. 13. (The pressure taps are located at the center of the base.) At small incidence, the base pressure dropped slightly with increasing angle of attack, and decreased slightly with increasing Reynolds number. But when the model was subjected to higher angles of attack, the base pressure rose noticeably, except at the lowest Reynolds number ($Re_{\infty,H} = 7000$). At the higher angles of attack ($> 17.5°$), flow separation on the leeward surface started to appear, and the surface pressure in the separated region became almost identical to the base pressure.

The reasons for the behavior of the base pressure as a function of angle of attack and Reynolds number are not clear. The base pressures on the wedges at zero angle of attack are scaled properly with the freestream Reynolds number as shown by Batt and Kubota,[6] for a number of wedge angles. For a given angle the boundary-layer thickness at the trailing edge is the proper scaling parameter. As may be seen from Fig. 13 this simple scaling does not hold anymore when the wedge is put at an angle of attack. At large angles of attack where separation occurs viscous-inviscid flow interaction on the leeward side and nose bluntness are important in establishing the plateau pressure after separation as shown by Hulcher and Behrens.[21] The plateau pressure was measured to be virtually the same as the base pressure. The correlation of base pressure for the same Reynolds number ($Re_{\infty,H} = 28{,}000$) but different model sizes are good, indicating that the aspect ratio AR (= span of model/base height) was also adequate for the large wedge ($AR = 16.7$) for the present experiments.

Near Wake Velocity Profiles

Figure 14 shows the near wake velocity profiles for the wedge at a Reynolds number of 55,000 at an angle of attack of 25°. The wake shocks are relatively weak on both sides. On the leeward side the velocity acceleration caused by the expansion waves is small, the velocity profiles have a relatively flat level in the inviscid region followed by a sharp drop in the viscous region, and the turning point clearly mark the location of shear layer edges. But on the windward side, the expansion waves about the trailing corner of the wedge are very strong; therefore, significant

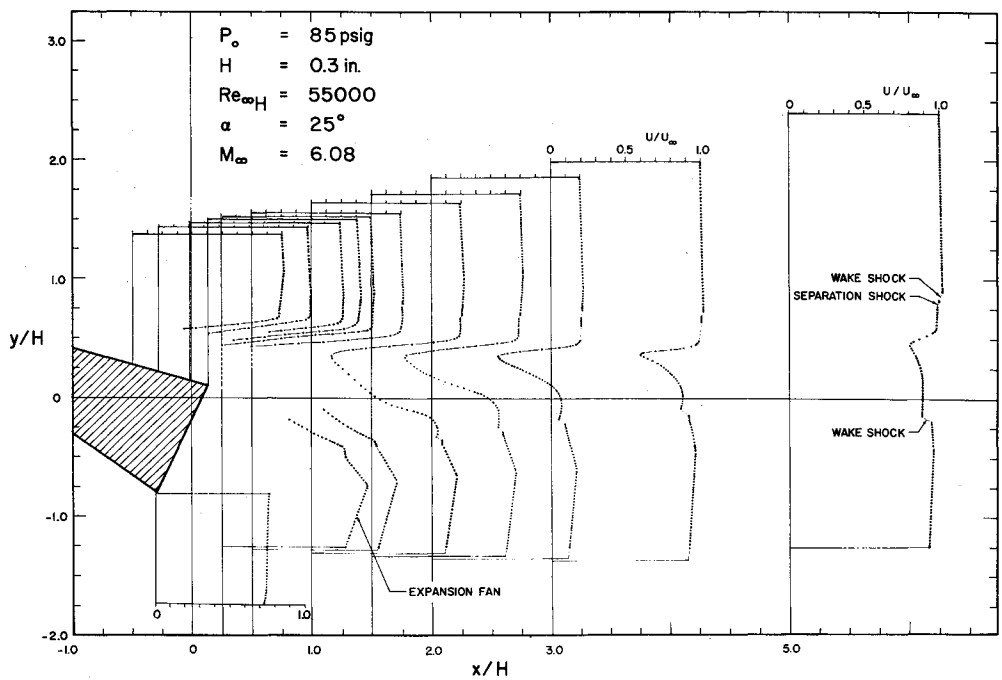

Fig. 14 Near wake velocity profiles of wedge at an angle of attack of 25°.

Table 1 Location of flow separation on leeward side surface of 20° wedges (% chord of separated flow measured from trailing edge)

H (in.)	0.15				0.30			
P_0 (psig)	10	35	60	85	10	35	60	85
$Re_{\infty_H} \times 10^{-4}$	0.7	1.4	2.1	2.8	1.4	2.8	4.1	5.5
M_∞ / Angle of attack α	6.02	6.04	6.06	6.08	6.02	6.04	6.06	6.08
17.5°		0		0	0	2	0	0
20.0	4%	4			5	5	6	7
22.5	10%	10		10	12	13	18	30
25.0	11%	14	20	25	20	34	36	40
27.0						45	60	63
30.0	30%	45	55	55				

transverse pressure gradients are noticeable just after the corner, and the flow is first accelerated inside the expansion fan toward the viscous wake, then decelerated due to shear stresses in the viscous wake and compression waves as the flow turns back toward nearly freestream direction. The shear layer edge on the windward side is defined as the point where the tangent of the maximum velocity gradient intersects the maximum velocity level. Part of the flow outside this viscous wake edge is coming from the boundary layer on the wedge (compare Fig. 14 with Fig. 15 which will be discussed in the next section), but viscous effects are very small for this flow that rapidly expanded about the wedge trailing corner, as shown by the fact that the total pressure is nearly constant along streamlines.

Flow Separation and Near Wake Flowfield

At small angles of attack, the structure of the near wake flow is very similar to that of the symmetric wake. The boundary layers separate at both trailing edges of the wedge and coalesce at about three-quarters of a base height downstream. As the angle of attack increases, the recirculation region moves toward the leeward side. When the angle of attack was increased beyond 17.5°, flow separation on the leeward surface was observed (see Table 1), and the recirculation region extended from the base to the leeward surface. Even though the oil flow technique does not yield very accurate results, it was observed (see Table 1) that separation moves upstream with increasing Reynolds number. This result is in agreement with findings in the laminar boundary-layer separation experiments on a flat plate at angle of attack[21] and on a ramp by Lewis et al.[22] and is also predicted theoretically by Lees and Reeves.[23]

The structure of typical near wake flowfields at an angle of attack of 25° is shown in Fig. 15. This figure shows some important features of the wake geometry, such as shock-wave location, shear layer edges, sonic line, contour of zero-velocity and streamlines. The contour of zero velocity is constructed from the points where pitot pressure is equal to static pressure.

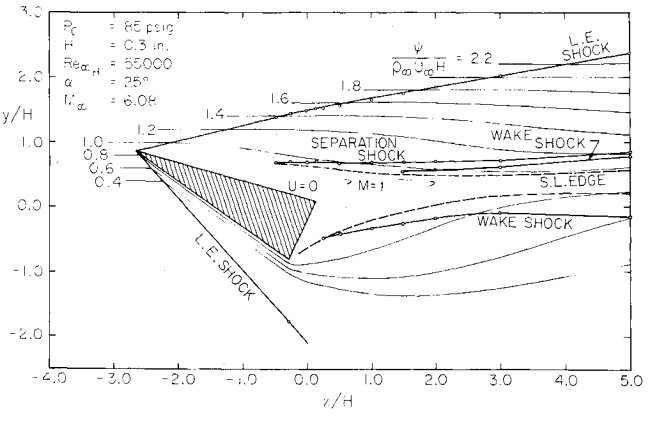

Fig. 15 Near wake flowfield of wedge at an angle of attack of 25°.

Note that the recirculation region is shorter as measured from the trailing corner of the wedge than at zero angle of attack[6] where the rear stagnation point was measured to be at $x/H \simeq 0.75$ at a wide range of Reynolds number. The streamline curvature near the windward trailing corner clearly indicates the strong pressure gradients in this region. At four or five base heights downstream of the base the flow in the viscous wake is again nearly parallel to the freestream direction as already found from the inviscid flow calculations.

Summary of Results

Experimental measurements of mean flow properties of hypersonic wakes behind wedges of 20° included angle were conducted at angles of attack up to 25° at Mach number 6, with freestream Reynolds number based on wedge base height ranging from 7000 to 55,000. The near and far wake flowfields were determined up to a downstream distance of 60 base heights.

Far Wake Flowfield

1) The overshoot in wake static pressure depends strongly on angle of attack; the higher the angle of attack, the larger the overshoot. The effect of Reynolds number on the overshoot follows the same trend as that for the symmetric wake; the lower the Reynolds number, the higher the overshoot. The effect of Reynolds number is very much smaller than that of angle of attack.

2) The viscous wake edge values of velocity, Mach number and temperature are very close to the freestream conditions for all angles of attack on the leeward side, and change considerably with angle of attack on the windward side. A weak expansion of the wake flow in the region behind the wake shocks changes the viscous wake edge conditions only very slowly as the flow moves downstream.

3) The inviscid wake flow parameters: wake static pressure, edge velocities, edge Mach numbers, edge temperatures and flow inclination in the real flow compare favorably with the simple inviscid shock expansion model for $M = 6$, $\alpha \leqq 25°$. The inviscid far wake flow is mainly determined by the relative strengths of the leading edge shocks and the fact that the flows at the edges of the viscous wake have to be nearly parallel to each other, with a weak dependence on the base flow. The viscous wake is accordingly affected by the differences in the inviscid flow on the windward and leeward sides.

4) In the laminar wake flows the wake widths, minimum velocities, minimum Mach numbers and maximum temperatures change very little with angle of attack. In the transitional wake flows, the sudden growth of wake width ("breakaway phenomenon") is observed, and indicates the onset of a nonlinear instability or transition.

5) The location of transition determined from the sudden increase of growth rate of wake thickness indicates that, for the same Reynolds number, transition moves upstream as the angle of attack is increased.

6) When wake flows are laminar, the velocity profiles at higher Reynolds number have much steeper gradients than those at the lower Reynolds number. Also, the maximum gradients of the flow profiles are steeper on the leeward side than on the windward side. The gradients increase with increasing angle of attack, explaining the increased instability of the wake and earlier transition. The fast decay of "wake component" in the transitional wake leaves profiles at $x/H = 60$ which are quite close to the profile shapes of a free shear layer.

7) Far wake streamlines are calculated. Viscous wake flow inclination is directed toward the leeward side. The dividing streamline has a larger slope with respect to freestream direction than the line of minimum velocity.

Laminar Near Wake Flow

1) At Reynolds number above $Re_{\infty_H} = 14{,}000$ the base pressure changes very little with angle of attack up to 10° but

changes strongly at higher incidences. At $Re_{\infty_H} = 7000$ the base pressure decreases with angle of attack up to 25°. Flow separation on the leeward surface starts to appear when the angle of attack is increased beyond 17.5°. The surface pressure in the separated region becomes almost identical to the base pressure.

2) When the wedge is at small angle of attack, the structure of the near-wake flow is very similar to that of the symmetric wake. The boundary layers separate at both trailing edges of the wedge and coalesce at about three quarters of a base height downstream. As the angle of attack increases, the recirculation region moves toward the leeward side of the wedge. When the angle of attack is increased beyond 17.5°, flow separation on the leeward surface is observed, and the recirculation region extends from the base to the leeward surface. The separation point on the leeward surface moves upstream with increasing Reynolds number.

References

[1] Lees, L., "Hypersonic Wakes and Trails," *AIAA Journal*, Vol. 2, No. 3, March 1964, pp. 417–428.

[2] Lykoudis, P. S., "A Review of Hypersonic Wake Studies," *AIAA Journal*, Vol. 4, No. 4, 1966, pp. 577–590.

[3] McCarthy, J. F., Jr. and Kubota, T., "A Study of Wakes behind a Circular Cylinder at $M = 5.7$," *AIAA Journal*, Vol. 2, No. 4, April 1964, pp. 626–629.

[4] Dewey, C. F., Jr., "Near Wake of a Blunt Body at Hypersonic Speeds," *AIAA Journal*, Vol. 3, No. 6, June 1965, pp. 1001–1010.

[5] Behrens, W., "Far Wake Behind Cylinders at Hypersonic Speeds: I. Flowfield," *AIAA Journal*, Vol. 5, No. 12, Dec. 1967, pp. 2135–2141; also "Far Wake behind Cylinders at Hypersonic Speeds: II. Stability," *AIAA Journal*, Vol. 6, No. 2, Feb. 1968, pp. 225–232.

[6] Batt, R. G. and Kubota, T., "Experimental Investigation of Laminar Near Wakes behind 20° Wedges at $M_\infty = 6$," *AIAA Journal*, Vol. 6, No. 11, Nov. 1968, pp. 2077–2083; also "Experimental Investigation of Far Wakes behind Two-Dimensional Slender Bodies at $M_\infty = 6$," *AIAA Journal*, Vol. 7, No. 11, Nov. 1969, pp. 2064–2071.

[7] Murman, E. M., "Experimental Studies of a Laminar Hypersonic Cone Wake," *AIAA Journal*, Vol. 7, No. 9, Sept. 1969, pp. 1724–1730.

[8] McLaughlin, D. K. et al., "Experimental Investigation of the Mean Flow of the Laminar Supersonic Cone Wake," *AIAA Journal*, Vol. 9, No. 3, March 1971, pp. 479–484.

[9] Pallone, A., Erdos, J., and Eckerman, J., "Hypersonic Laminar Wakes and Transition Studies," *AIAA Journal*, Vol. 2, No. 5, May 1964, pp. 855–863.

[10] Reeves, B. L. and Lees, L., "Theory of Laminar Near Wake of Blunt Bodies in Hypersonic Flow," *AIAA Journal*, Vol. 3, No. 11, Nov. 1965, pp. 2061–2074.

[11] Weiss, R. F., "A New Theoretical Solution of the Laminar Hypersonic Near Wake," *AIAA Journal*, Vol. 5, No. 12, Dec. 1967, pp. 2142–2149.

[12] Henderson, A., Jr., "Shuttle Technology for Aerothermodynamics," *Astronautics and Aeronautics*, Vol. 9, No. 2, Feb. 1971, pp. 26–36.

[13] Tracy, R. R., "Hypersonic Flow over a Yawed Circular Cone," Memo 69, Aug. 1, 1963, Hypersonic Research Project, Graduate Aeronautical Labs., California Inst. of Technology, Pasadena, Calif.

[14] McLaughlin, D. K., "Experimental Investigation of the Stability of the Laminar Supersonic Cone Wake," *AIAA Journal*, Vol. 9, No. 4, April 1971, pp. 696–702.

[15] Kahane, A. and Lees, L., "The Flow at the Rear of a Two-Dimensional Supersonic Airfoil," *Journal of Aeronautical Sciences*, Vol. 15, No. 3, March 1948, pp. 167–170.

[16] Wu, J. J., "An Experimental Study of Hypersonic Wakes behind Wedges at Angle of Attack," Ae.E. thesis, 1971, California Inst. of Technology, Pasadena, Calif.

[17] Behrens, W., "Viscous Interaction Effects on a Static Pressure Probe at $M = 6$," *AIAA Journal*, Vol. 1, No. 12, Dec. 1963, pp. 2364–2366.

[18] McCarthy, J. M., Jr., "Hypersonic Wakes," Memo 67, July 2, 1962, Hypersonic Research Projects, Graduate Aeronautical Labs., California Inst. of Technology, Pasadena, Calif.

[19] Michalke, A. and Schade, H., "Zur Stabilität von Freien Grenzschichten," *Ingenieur-Archiv*, Vol. 23, No. 1, 1963, pp. 1–23.

[20] Kubota, T. and Behrens, W., "Linear Instability of Far Wake Flow," *AIAA Journal*, Vol. 8, No. 6, June 1970, pp. 1178–1179.

[21] Hulcher, G. D. and Behrens, W., "Viscous Hypersonic Flow Over a Flat Plate at Angle of Attack with Leeside Boundary Layer Separation," Proceedings of the 1972 Heat Transfer and Fluid Mechanics Institute, edited by R. B. Landis and G. J. Hordemann, Stanford University Press, Stanford, Calif., 1972.

[22] Lewis, J. E., Kubota, T., and Lees, L., "Experimental Investigation of Supersonic Laminar, Two-Dimensional Boundary-Layer Separation on a Compression Corner with and without Cooling," *AIAA Journal*, Vol. 6, No. 1, Jan. 1968, pp. 7–14.

[23] Lees, L. and Reeves, B. L., "Supersonic Separated and Reattaching Laminar Flows: General Theory and Application to Adiabatic Boundary Layer-Shock Wave Interactions," *AIAA Journal*, Vol. 2, No. 11, Nov. 1964, pp. 1907–1920.